# Synthesis of Mesostructured Nickel Oxide with Silica

**Xinghua Liu,[†] C.-M. Chun,[‡] Ilhan A. Aksay,[‡] and Wei-Heng Shih*,[†]**

*Department of Materials Engineering, Drexel University, Philadelphia, Pennsylvania 19104, and Department of Chemical Engineering and Princeton Materials Institute, Princeton University, Princeton, New Jersey 08544-5263*

Mesostructured nickel oxide was formed with nickel sulfate and cationic surfactant cetyltrimethylammonium bromide (CTAB). X-ray diffraction (XRD) peaks at low scattering angles and transmission electron microscopy (TEM) indicated that a mesostructure was formed. However, these XRD patterns disappeared after calcination. The addition of sodium silicate in the precursor solutions produced a mesostructure, which is stable against calcination. Surface areas as high as 530 $m^2/g$ can be obtained for the nickel silicate mesophase. TEM-EDXS showed that the Si/Ni molar ratio in the mesophase is ∼0.5, independent of the initial Si/Ni ratio in the precursor.

## Introduction

Mesoporous silica, which was discovered by researchers at Mobil,[1] contains periodic pore structures with uniform pore sizes ranging from 20 to 100 Å. The larger pore size than that of zeolites makes the mesoporous materials a good candidate as catalyst supports, molecular sieves, and adsorbents. Since the discovery of mesoporous silica, many researchers have investigated the synthesis of mesoporous materials other than silicates such as transition metal oxides, which are desirable for catalytic applications. Several synthetic pathways[2−4] have been studied: $S^+I^-$, $S^-I^+$, $S^+X^-I^+$, $S^-X^+I^-$, where S indicates the surfactant; I, the inorganic ion; and X, the mediating ion. In general, using ionic surfactants such as cetyltrimethylammonium bromide (CTAB), hexagonal mesoporous phase (MCM-41) was produced. On the other hand, using neutral surfactant, i.e., $S^0I^0$, Pinnavaia et al.[3,5] synthesized mesoporous molecular sieves, which are different from MCM-41. Additional mesoporous materials that differ from MCM-41were discovered over the years,[6−13] and will be mentioned in the next paragraph. To include phases that have structure similar to the MCM-41 before the removal of surfactant, we call all materials with mesoscale structure mesostructured materials. Mesostructured materials include the mesoporous materials such as MCM-41 and nonsilicate materials.

Several mesostructured nonsilicates have been synthesized in the past. Abe et al.[7] synthesized vanadium−phosphorus mixed-oxide mesostructures. Antonelli and Ying[8] synthesized mesostructured $TiO_2$ using titanium acetylacetone isopropoxide precursors and aliphatic phosphate surfactants. One of the difficulties encountered in the synthesis of transition metal oxides is that the mesostructured phase is not stable during calcination. The periodic structure is destroyed during heat treatment. Stabilization or strengthening of the periodic structure is needed. Sayari et al.[9] synthesized stable mesoporous $ZrO_2$ using zirconium sulfate and CTAB, followed by dispersing the formed $ZrO_2$ in $KH_2PO_4$ solution. The introduction of phosphate into the zirconium oxide stabilized the mesostructure against calcination. Antonelli and Ying[10] synthesized hexagonally packed mesostructured tantalum oxide using a novel approach involving the hydrolysis of long-chain primary amine complexes of $Ta(OEt)_5$. The inorganic precursor is covalently bonded to the template and thus enhances the thermal stability of the mesostructure. More recently synthesized mesostructured oxides include hafnium oxide,[11] niobium oxide,[12] and manganese oxide.[13] In another approach, Vaudry et al.[14] synthesized pure alumina mesoporous materials using aluminum alkoxide and carboxylic acids with controlled amounts of water in low molecular weight alcoholic solvent. Yada et al.[15] synthesized hexagonal mesoporous aluminum oxide using dodecyl sulfate surfactants. Therefore, it is also possible to obtain stable nonsilicate mesostructures by choosing the appropriate surfactant and controlling the chemical reactions between the inorganic and organic species.

In this paper, we investigated the synthesis of mesostructured nickel oxide, which has been shown to be an excellent electrode material for energy storage applications.[16] The stabilization of the mesostructure is especially critical for divalent elements such as Ni, which does not form a network structure like the silicates. The lack of a network-forming multivalent bond is probably the reason that no stable mesoporous oxides have been synthesized for divalent elements yet. Recently Stein et al.[17] used the tetraethyl orthosilicate (TEOS) to provide a framework structure for the synthesis of niobotungstate salts. In the present study, by using an ionic surfactant, it was found that the synthesized nickel oxide showed similar X-ray diffraction (XRD) patterns as the pure aluminum oxide mesoporous materials.[14] However, heat treatment destroyed the structures and the low-angle Bragg peaks disappeared. Since silica can form network structure and easily form the hexagonal mesoporous phase (MCM-41), we investigated the effect of adding silicate in strengthening the nickel oxide mesostructure.

## Experimental Procedure

The synthesis procedure started with preparing a 25 wt % aqueous cetyltrimethylammonium bromide $[CH_3(CH_2)_{15}N(CH_3)_3Br]$ (CTAB) solution and stirring for 5 min. Nickel(II) sulfate hexahydrate $[NiSO_4·6H_2O]$

[†] Drexel University.
[‡] Princeton University.

10.1021/ie990129l CCC: $19.00 
Published on Web 02/04/2000

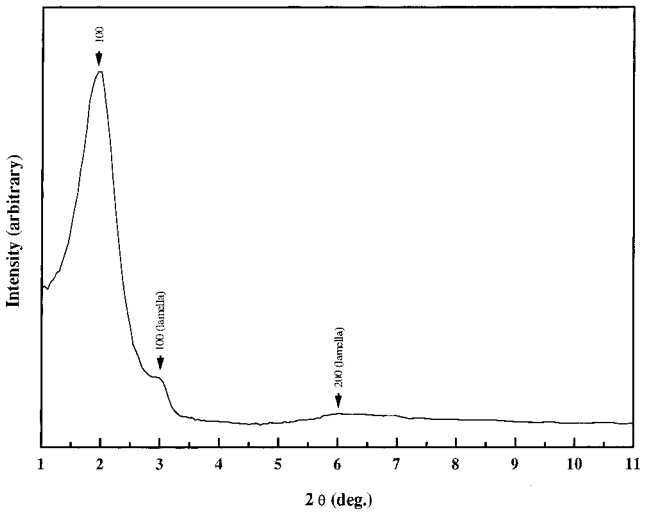


**Figure 1.** XRD patterns of as-synthesized precipitates from $NiSO_4$−CTAB solutions.

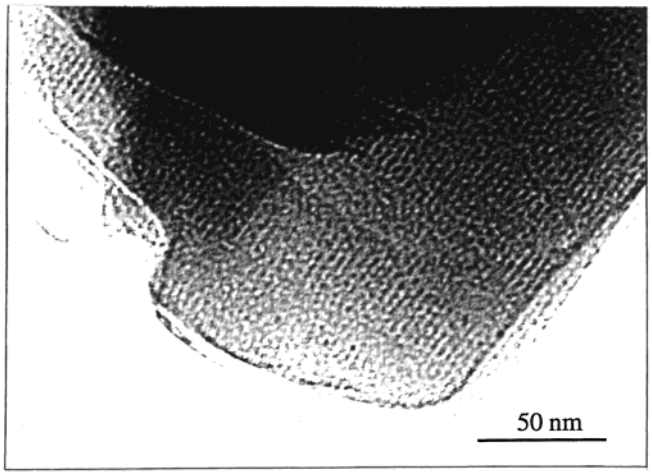


**Figure 2.** TEM micrograph of as-synthesized precipitates from $NiSO_4$−CTAB solutions.

(Aldrich) was added to the surfactant solution with the desired surfactant/$NiSO_4$ molar ratio. When sodium silicate is needed, the appropriate amount of sodium silicate (Soluble Silicate N with the composition, 28.7 wt % $SiO_2$, 8.9 wt % $Na_2O$, 62.4 wt % $H_2O$) from PQ Corporation was added to the $NiSO_4$−CTAB solution such that appropriate $SiO_2/NiSO_4$ molar ratio was retained. More water was then added to adjust the surfactant concentration to 2 wt % and the solution was stirred for 5 min. The pH value of solutions was adjusted with HCl (1 M) or $NH_4OH$ (29 wt %). The solution (pH $\approx$ 7−8) was heat treated at 115 °C in an autoclave for 20 h. The sediments were washed with distilled water and separated out by centrifugation. The samples were dried at 60−80 °C for at least 8 h. As-synthesized samples were calcined at 500 °C in air for 2 h to remove surfactant.

X-ray diffraction (XRD) was carried out using a Siemens D500 diffractometer with Cu Kα radiation ($\lambda$ = 0.154 nm). The scan step was 0.05° with a step time of 6 s for the low-angle analysis and the scan step was 0.05° with a step time of 0.5 s for the high-angle analysis. AMRAY 1830 scanning electron microscope was used to perform EDXS (energy dispersion X-ray spectroscopy) at 30 kV, ZAF quantitative method was used to calculate the amount of Ni, Si, S, and O.

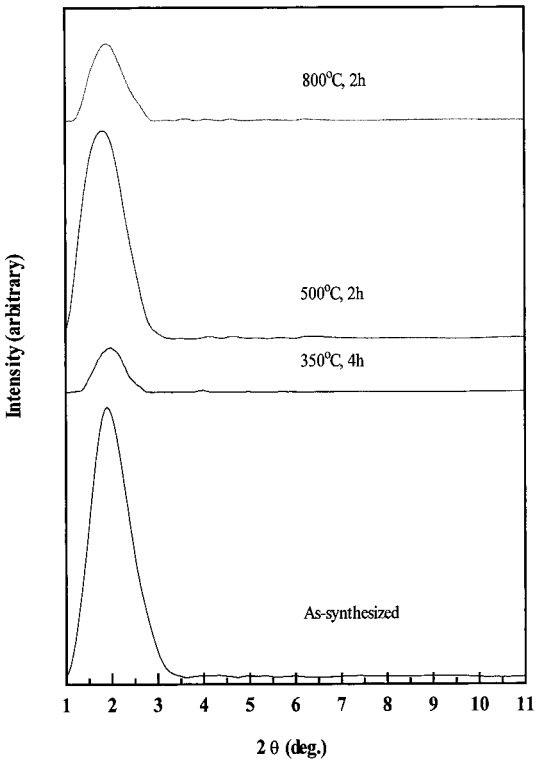


**Figure 3.** XRD patterns of calcined precipitates from $NiSO_4$−CTAB−sodium silicate precursor solutions with surfactant/$NiSO_4$ = 0.2 and Si/Ni = 0.21.

Standards were used for calibration before the experiment. JEOL JEM-4000EX was used to perform transmission electron microscopy (TEM). The structure, size, morphology, and local chemical composition of mesostructured nickel silicates were examined by analytical transmission electron microscopy (CM200 FEG, Philips Electronics) attached with an EDXS (PGT 2000, Princeton Gamma Tech.). EDXS analysis was typically performed at an accelerating voltage of 200 keV with a 12 nm spot size. TEM samples were prepared by dipping a Cu TEM grid, coated with holey carbon film, into a colloidal suspension of particles dispersed in methanol which were then air-dried and stored in a vacuum chamber. Differential scanning calorimeter (DSC) was performed on PERKIN ELMER DSC7. Thermogravimetric analyses (TGA) were performed on a Du Pont 951 thermogravimetric analyzer. The samples were heated in air at a rate of 10 °C/min for both DSC and TGA measurement. Infrared spectra were recorded on a PERKIN-ELMER 1600 series FTIR spectrometer using KBr pellet techniques. A typical pellet contains about 1 wt % sample in KBr. Nitrogen adsorption/desorption experiments were carried out at 77 K on a NOVA 2200 analyzer. Surface areas were calculated from the isotherm data using the BET (Brunauer, Emmet, and Teller) equation.[18] The pore size distributions were calculated using the Barret−Joyner−Hallender (BJH) method[19] using the desorption isotherm data.

## Results and Discussion

Figure 1 shows the XRD patterns of precipitates obtained from the mixtures of $NiSO_4$ and CTAB surfactant with the CTAB/$NiSO_4$ molar ratio = 0.2. The as-synthesized sample exhibits a dominant peak near $2\theta$ = 2°, which corresponds to a $d_{100}$ spacing of 46 Å.

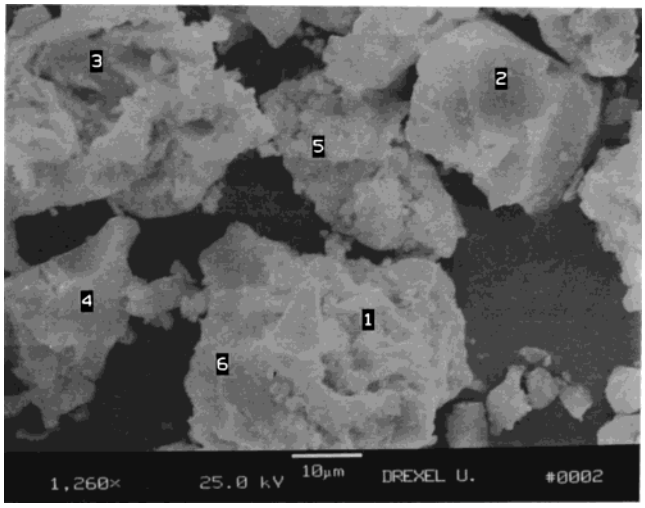


| Location | Chemical Composition Measured by SEM EDXS (atom%) | | | | |
|---|---|---|---|---|---|
| | O | S | Si | Ni | Si/Ni |
| 1 | 74.71 | 0 | 13.99 | 11.31 | 1.24 |
| 2 | 35.12 | 0 | 37.12 | 27.76 | 1.34 |
| 3 | 58.19 | 0 | 18.53 | 23.28 | 0.80 |
| 4 | 38.85 | 0 | 22.66 | 38.49 | 0.59 |
| 5 | 52.87 | 0 | 19.52 | 27.61 | 0.71 |
| 6 | 70.30 | 0 | 15.46 | 14.24 | 1.09 |

**Figure 4.** The SEM micrograph of the precipitates from $NiSO_4$−CTAB−sodium silicate precursor solutions with surfactant/$NiSO_4$ = 0.2 and Si/Ni = 0.21. The chemical compositions of several particles are included.

The small hump near $2\theta = 3°$ and the broad peak at $2\theta = 6°$ are interpreted as the (100) and (200) peaks of a lamella phase. The coexistence of a mesophase and a lamella phase is a common feature in mesoporous materials synthesis. The qualitative feature of the XRD pattern in Figure 1 is similar to that of the mesoporous aluminum oxide synthesized by Vaudry et al.[14] TEM was performed on the precipitates from $NiSO_4$−CTAB solutions. The TEM micrograph of precipitates is shown in Figure 2, indicating the existence of a periodic structure. From the results of Figures 1 and 2, it is concluded that a periodic, organic/inorganic composite phase containing Ni can be synthesized. However, after calcination at 500 °C for 2 h, the low-angle Bragg peaks disappeared, indicating the breakdown of the periodic structure.

The results in Figure 1 indicate that mesostructured phase can be formed in the $NiSO_4$−CTAB solutions but it is not stable against the heat treatment. To stabilize the mesostructured phase, we added small amounts of sodium silicate in the $NiSO_4$−CTAB solutions. Figure 3 shows the XRD patterns of precipitates obtained from the sodium silicate, $NiSO_4$, and CTAB mixtures and heat-treated at elevated temperatures. The surfactant/$NiSO_4$ molar ratio was kept at 0.2 and $SiO_2/NiSO_4$ molar ratio was 0.21. The addition of $SiO_2$ produced a mesostructured phase, which is stable against heat treatment up to 800 °C for 2 h. Furthermore, when heat-treated at 350 °C for 4 h, the low-angle peak intensity decreased. On the other hand, when heat-treated at 500 °C for 2 h, the low-angle peak intensity increased. Heat

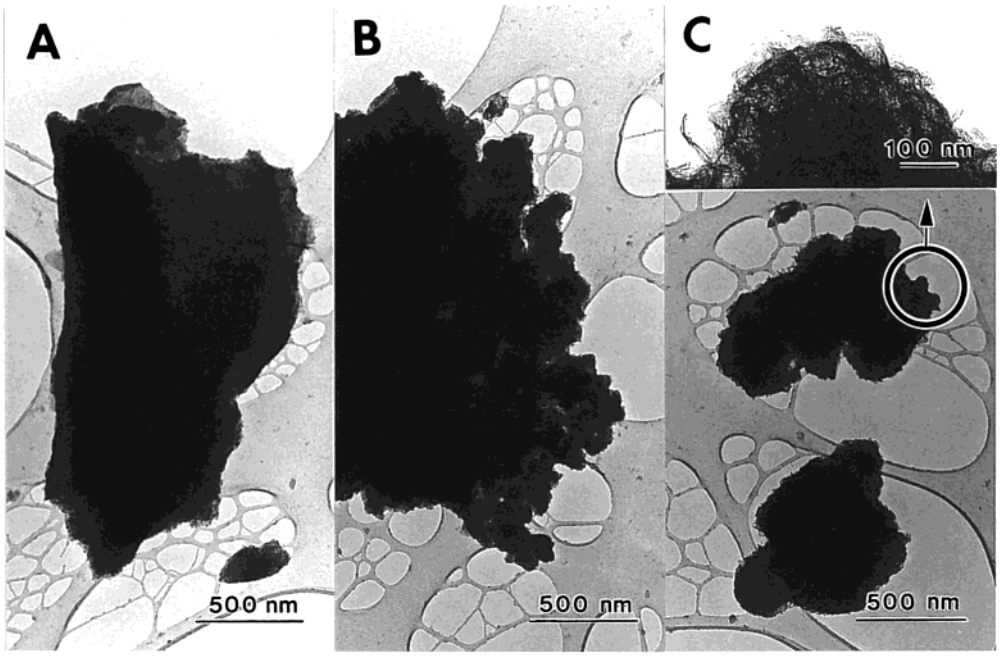


| Average Chemical Compostion Measured by TEM EDXS (atom%) | | | |
|---|---|---|---|
| Element | A. Platelet | B. Spherical chunk | C. Fibril aggregates |
| Ni | 65.8±1.9 | 83.0±3.7 | 99.7±0.4 |
| Si | 30.3±1.8 | 14.9±3.3 | 0.0±0.0 |
| S | 3.9±0.9 | 2.1±0.4 | 0.3±0.4 |
| Si/Ni | 0.46±0.04 | 0.18±0.04 | 0.00±0.00 |

* Used Phillips CM200/FEG, operated at 200 Kev with the spot size of 12 nm at various particles

**Figure 5.** The TEM image of supernatant of calcined precipitates from $NiSO_4$−CTAB−sodium silicate precursor solutions with surfactant/$NiSO_4$ = 0.2 and Si/Ni = 0.21 dispersed in ethanol. The chemical compositions of different morphologies are included.

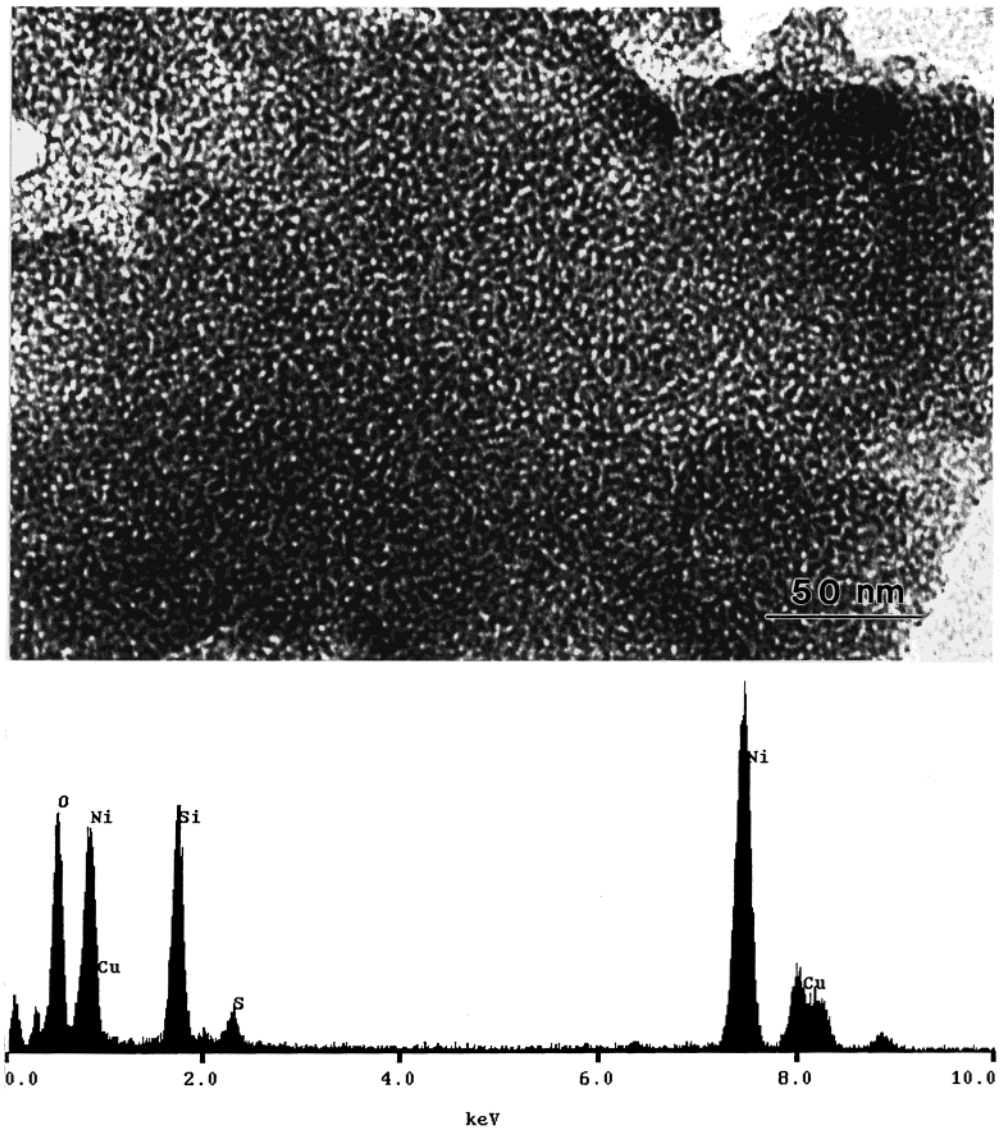


| Chemical Composition Measured by TEM EDXS (atom%) | | | | | | | | |
|---|---|---|---|---|---|---|---|---|
| Element | spot 1 | spot 2 | spot 3 | spot 4 | spot 5 | spot 6 | spot 7 | average |
| Ni | 64.7 | 63.8 | 63.4 | 66.5 | 67.5 | 68.7 | 65.8 | 65.8±1.9 |
| Si | 32.4 | 31.8 | 31.7 | 29.7 | 29.9 | 27.3 | 29.2 | 30.3±1.8 |
| S | 2.9 | 4.4 | 4.9 | 3.8 | 2.6 | 4.0 | 5.0 | 3.9±0.9 |
| Si/Ni | 0.5 | 0.5 | 0.5 | 0.45 | 0.44 | 0.40 | 0.44 | 0.46±0.04 |

* Used Phillips CM200/FEG, operated at 200 Kev with the spot size of 12 nm at various particles

**Figure 6.** The TEM image of the mesophase from $NiSO_4$−sodium silicate−CTAB solutions. The chemical composition analysis shows the mesophase has Si/Ni ≈ 0.5.

treatment at even higher temperature of 800 °C at 2 h, the intensity decreased again. The behavior of the low-angle peak intensity correlates well with the specific surface area data that will be presented later.

The precipitates from the sodium silicate−$NiSO_4$−CTAB solution with CTAB/$NiSO_4$ = 0.2 and Si/Ni = 0.21 were examined by SEM, and the results are shown in Figure 4 together with the chemical compositions of several large clusters in the micrograph. The chemical compositions were measured by the EDXS probe in the SEM with a probe size of 5 $\mu$m. The oxygen content varies significantly because of the presence of oxygen from the atmosphere. Even though the individual concentrations of Si and Ni may not be absolutely accurate due to the error in oxygen content, the Si/Ni molar ratios are relatively accurate. There is a distribution of Si/Ni molar ratios in the precipitates. The measured Si/Ni ratio ranges from 0.59 to 1.34 with a mean value of 0.96. The mean value of Si/Ni ≈ 1 is consistent with the overall Si/Ni ratio of 1.0 measured from a large probe area covering more than 0.4 $mm^2$. The mean Si/Ni ratio of 1.0 in these precipitates is higher than the original Si/Ni ratio in the solution of 0.21. This indicates that some Ni species remained in the solution while Si occurred mostly in the precipitate. The distribution of Si/Ni ratio can be understood by considering how the $SiO_4$ tetrahedra connect each other. If all the four corners of neighboring $SiO_4$ tetrahedra are linked together through Ni, this is similar to the olivine structure which has a Si/Ni = 0.5. However, if

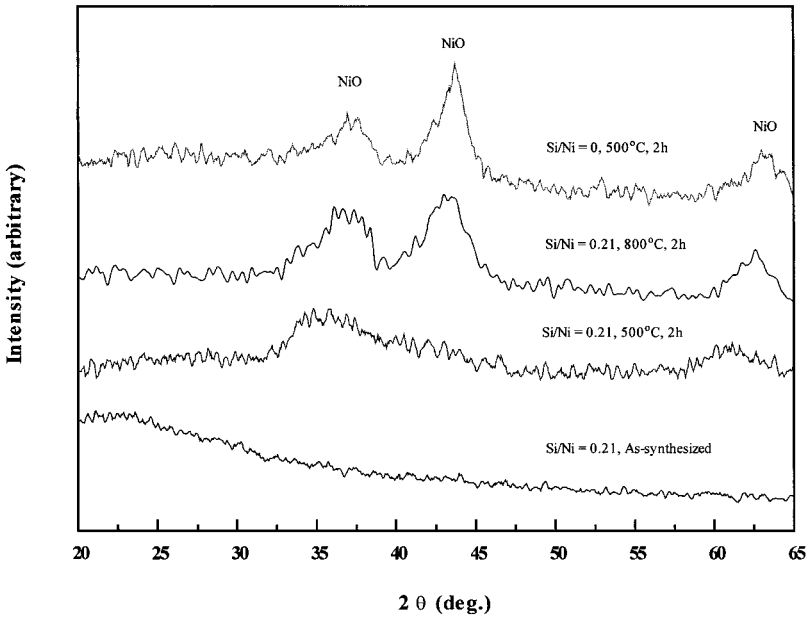


**Figure 7.** XRD patterns of precipitates prepared from $NiSO_4$−CTAB−sodium silicate precursor solutions with surfactant/$NiSO_4$ = 0.2 and Si/Ni = 0.21 at large scattering angles. The XRD patterns for the sample without the addition of sodium silicate is also included for comparison.

**Table 1. Properties of Silica Stabilized Mesostructured Nickel Oxide**

| CTAB/$NiSO_4$ (molar ratio) | $SiO_2$/$NiSO_4$ (molar ratio) | $H_2O$/$NiSO_4$ (molar ratio) | $d_{100}$ spacing (Å) | | | BET surface area after 500 °C calcination ($m^2$/g) |
|---|---|---|---|---|---|---|
| | | | as-synthesized | 350 °C, 4 h | 500 °C, 2 h | |
| 0.1 | 0 | 200 | 44.39 | no peak | no peak | 31 |
| 0.1 | 0.05 | 200 | 44.13 | 42.73 | no peak | not measured |
| 0.1 | 0.10 | 200 | 44.24 | 42.21 | no peak | not measured |
| 0.1 | 0.17 | 200 | 46.44 | 45.22 | 47.68 | 377.2 |
| 0.2 | 0.10 | 200 | 43.12 | no peak | no peak | not measured |
| 0.2 | 0.21 | 200 | 46.38 | 46.53 | 48.28 | 529.1 |
| 0.2 | 0.34 | 200 | 43.55 | 44.31 | 43.34 | 516.1 |
| 0.2 | 0.50 | 200 | 43.38 | 45.23 | 44.14 | 467.6 |

three of the four corners of the $SiO_4$ tetrahedra are linked together through Ni and the remaining corner is linked directly with Si−O−Si bond, then Si/Ni = 0.67. Similarly, if two corners of $SiO_4$ tetrahedra are linked through Ni and two with Si−O−Si bond, Si/Ni = 1. When only one corner linked through Ni, Si/Ni = 2. Therefore, the distribution of Si/Ni is expected to vary from 0.5 to 2, which is consistent with the observation of 0.59 to 1.34. If all the cases have equal probability, the average Si/Ni ratio would be 1.04, which is very close to 0.96 observed in Figure 4. It should be noted that these speculated structures are amorphous while the olivine structure is crystalline. Alternatively, it may be argued that there may be mixtures of Ni and Si species that give rise to the Si/Ni ratios that we observed. To gain further insight, TEM-EDXS study was performed.

The TEM samples were prepared by suspending the calcined precipitates from the sodium silicate−$NiSO_4$−CTAB solution with CTAB/$NiSO_4$ = 0.2 and Si/Ni = 0.21 in ethanol and the TEM grid was dipped in the supernatant of the suspension. There were significant amounts of sediment in the ethanol suspensions. The TEM was performed on the suspended particles only. These particles were typically on the order of 1 $\mu$m in size, which is significantly smaller than the clusters examined in the SEM. As shown in Figure 5, regions of different morphologies were found in the suspended particles. The platelet morphology (Figure 5A) corresponds to the mesophase with an average Si/Ni = 0.46 as measured by the EDXS. Detailed images and the

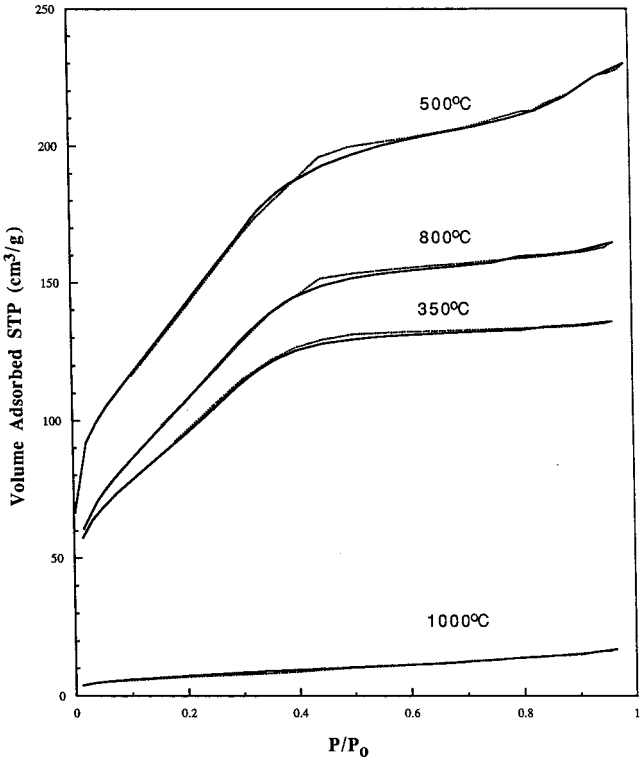


**Figure 8.** The $N_2$ adsorption and desorption isotherms of the calcined mesostructured nickel silicate prepared at surfactant/$NiSO_4$ = 0.2 and Si/Ni = 0.21 at elevated temperatures.

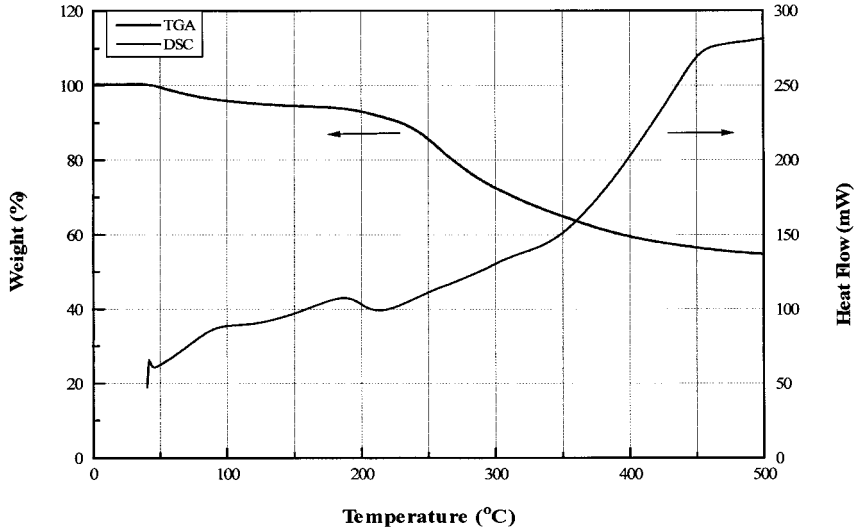


**Figure 9.** TGA and DSC results of mesostructured nickel silicate prepared at surfactant/$NiSO_4$ = 0.2 and Si/Ni = 0.21.

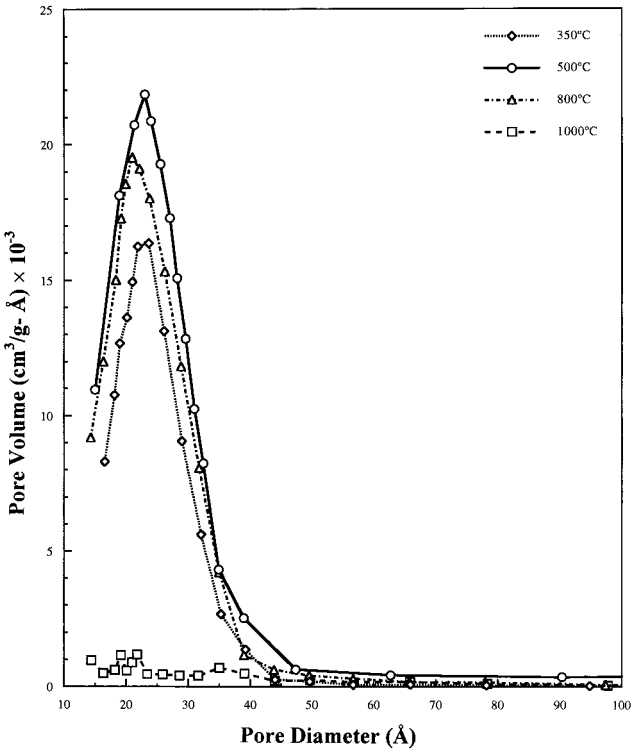


**Figure 10.** The pore size distribution of mesostructured nickel silicate prepared at surfactant/$NiSO_4$ = 0.2 and Si/Ni = 0.21 at elevated temperatures.

**Table 2. Properties of the Sample with CTAB/$NISO_4$ = 0.2 and $SiO_2$/$NiSO_4$ = 0.21 Calcined at Various Temperatures for 2 h**

| $T$ (°C) | $d_{100}$ spacing (Å) | BET surface area ($m^2$/g) | average pore diameter (nm) |
|---|---|---|---|
| 350 | 46.5 | 354.1 | 2.4 |
| 500 | 48.3 | 529.1 | 2.8 |
| 800 | 46.3 | 405.3 | 2.5 |
| 1000 | no peak | 25.9 | |

distribution of Si/Ni ratios will be shown later. The spherical chunks (Figure 5B) are Ni-rich phases with Si/Ni = 0.21, similar to the initial ratio in the precursor. The fibril aggregates (Figure 5C) correspond to even higher Ni content. Note that the chemical analysis were done for the three elements Ni, Si, and S only. The fibril aggregates are not pure Ni but are likely nickel oxide since oxygen was not measured. Therefore, combining the results of TEM-EDXS and SEM-EDXS, there are Si-rich phases and Ni-rich phases coexisting with the mesophase in the precipitates of sodium silicate−$NiSO_4$−CTAB. Figure 6 shows the high magnification of TEM image of the mesophase together with the results of EDXS analysis. The mesophase is clearly disordered but with uniform pore size. The chemical composition distribution was measured with the EDXS probe with a spot size of 12 nm. The variations of the chemical composition are also shown in Figure 6 for seven different locations. The Si/Ni ratio in the mesophase is shown to be quite uniform. The results in Figure 6 indicate that Si and Ni are microscopically mixed in the mesophase.

The differences in the chemical compositions of particles found in the supernatant and in the sediment of the ethanol suspensions of precipitates from sodium silicate−$NiSO_4$−CTAB solution are further investigated in a separate SEM study. It was found that the morphology of particles in the supernatant is platelet with an average Si/Ni ≈ 0.34. On the other hand, the morphology of particles in the sediment shows clusters with an average Si/Ni ≈ 0.95. Therefore, the chemical composition of particles in the supernatant is indeed different from that of the sediment, as seen in the different results between TEM and SEM. The platelet morphology of the suspended particles seen in SEM is probably due to the mesophase. On the other hand, the Si-rich particles tend to aggregate and settle to the bottom of the suspension.

To verify whether the $NiSO_4$ participated in the formation of the mesophase or not, sodium silicate was mixed with the CTAB surfactant in the same condition as in Figures 3−6 except no $NiSO_4$ was added. The XRD pattern of the precipitate showed only lamella phase with a $d_{100}$ spacing of 24 Å, which disappeared after calcination. Therefore, the sodium silicate used in the synthesis cannot form the mesophase alone. Clearly, the $NiSO_4$ is needed for the formation of the mesostructured phase, which results from the interaction among the sodium silicate, $NiSO_4$, and CTAB surfactant. This result is consistent with the finding in Figure 6 that Si and Ni are intimately mixed in the mesophase.

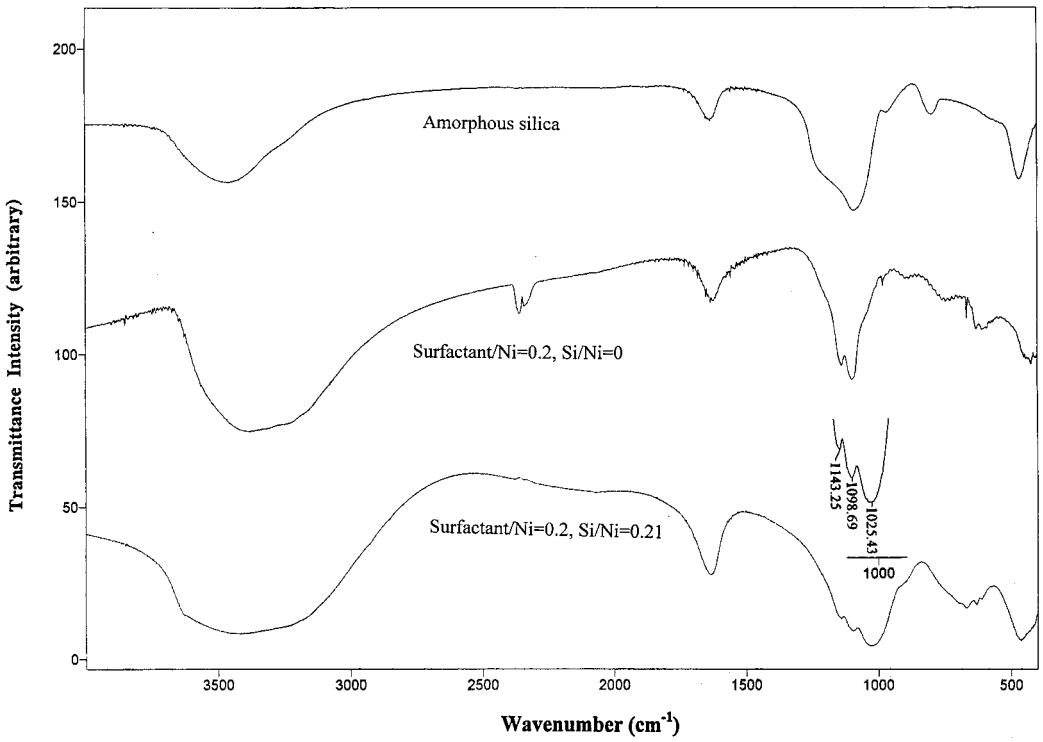


**Figure 11.** Infrared spectra for (a) amorphous silica without nickel oxide, (b) nickel oxide without silicate (surfactant/Ni = 0.2, Si/Ni = 0.), and (c) mesostructured nickel silicate (surfactant/Ni = 0.2, Si/Ni = 0.21).

The TEM of the mesophase obtained from CTAB/$NiSO_4$ = 0.2 and Si/Ni = 0.34 has also been studied. This is done to investigate whether the initial Si/Ni ratio affects the chemical composition of the mesophase. It was found that the Si/Ni molar ratio in the mesophase is also ~0.5, similar to that of mesophase precipitated from an initial Si/Ni = 0.21 precursors. This result indicates that the mesophase has a well-defined chemical composition independent of the initial Si/Ni molar ratios in the precursor.

In the phase diagram of $SiO_2$ and NiO, there is an equilibrium phase, $2NiO{\cdot}SiO_2$, which has an olivine structure. The Si/Ni molar ratio of 0.5 for the mesophase indicates that the mesophase may be a disordered olivine phase. The olivine structure is made up of oxygen atoms in a hexagonal close-pack arrangement and the Ni atoms occupied half of the octahedral sites and the Si atoms occupies one-eighth of the tetrahedral sites. On the other hand, pure NiO has the rocksalt structure. It is possible that the small amount of Si atoms added occupy the tetrahedral sites in the rocksalt structure and at the same time distort the structure of NiO, giving rise to a disordered phase. We speculate that the mesophase probably has a network structure of $SiO_4$ tetrahedra linked together by Ni atoms on every corners. More work needs to be done to confirm this speculation.

The XRD patterns of the precipitates prepared with surfactant/$NiSO_4$ = 0.2 and Si/Ni = 0.21 at large scattering angles are shown in Figure 7. The XRD pattern of the sample without the addition of sodium silicate is also included for comparison. NiO phase appeared at 500 °C in both cases. However, the intensity of the diffraction peaks of the NiO phase of the sample with silicates is much weaker than that of the sample without silicates. Apparently, the addition of sodium silicate suppresses the degree of crystallinity of NiO at 500 °C. Strong NiO peaks occur at 800 °C for the sample with silicates.

The amount of sodium silicate added was varied, and its effect on the formation of the mesophase was studied. The results are summarized in Table 1. Without the addition of sodium silicate, the low-angle Bragg peak of the mesophase disappeared after heat treatment at 350 °C for 4 h. When sodium silicate was added and the Si/Ni molar ratio increased, the low-angle Bragg peak survived at 350 °C although it disappeared at 500 °C. Increasing the Si/Ni molar ratio in the solution to 0.17, the mesophase remained after heat treatment at 500 °C for 2 h. Therefore, the addition of sodium silicate can produce a stable mesophase when the Si/Ni molar ratio is higher than a threshold, which is 0.17 in the case of the surfactant/Ni molar ratio = 0.1. When the surfactant/$NiSO_4$ molar ratio in the solutions was increased to 0.2, the Si/Ni molar ratio of 0.1 could not generate a stable mesophase up to 350 °C, in contrast to the case when surfactant/$NiSO_4$ molar ratio = 0.1. This result implies that when the amount of surfactant in the solution increases, the Si/Ni threshold needed for the formation of mesophase also increases. We could qualitatively argue that when more surfactant is added, more Ni will be incorporated in the precipitate therefore the amount of Si needed to stabilize the structure must be higher.

For the case of surfactant/Ni molar ratio = 0.2, three Si/Ni ratios of precursors were studied, including Si/Ni = 0.5. As shown in Table 1, the Si/Ni = 0.21 gives the highest surface area while Si/Ni = 0.5 the smallest. Since the mesophase has a composition of Si/Ni ≈ 0.5, it was thought that an initial Si/Ni = 0.5 would give the highest surface area. However, this is not the case. As shown in Figure 5, there are several other phases formed besides the mesophase. Therefore, it is not surprising that Si/Ni = 0.5 did not give the largest

amount of the mesophase. Clearly the initial Si/Ni molar ratio in the precursor is not the only controlling parameter in the process.

The nitrogen adsorption/desorption behavior of the mesoporous materials was studied with a BET surface area analyzer. The adsorption and desorption isotherms of the precipitate with surfactant/$NiSO_4$ = 0.2 and Si/Ni = 0.21 and calcined at several temperatures are shown in Figure 8. The adsorption isotherms are very similar to that of mesoporous aluminum oxide[14] and the specific surface area is similar to that of $ZrO_2$ mesoporous phase with phosphate.[9] Note that the adsorbed amount of nitrogen gas by the precipitate heat treated at 500 °C is the highest. The corresponding surface area for the precipitates treated at various temperatures are summarized in Table 2. The specific surface area increases and then decreases with increasing treatment temperature and this trend is similar to that found in the low-angle Bragg peak intensity, as shown in Figure 3. The specific surface area is correlated with the XRD intensity. In other words, higher XRD intensity correlates with larger specific surface area. TGA analysis was performed up to 500 °C. It was found that the weight loss from 200 to 500 °C is about 30%, in agreement with the amount of surfactant in the sample. Very little weight loss occurred above 500 °C. DSC measurement was also performed and the results after 500 °C show very little heat flow, in agreement with the TGA results. Figure 9 shows the TGA and the DSC results. The significant weight loss between 300 and 500 °C indicates that there is still some occluded organic materials in the system at 350 °C. Not until 500 °C, the organic materials are removed resulting in a larger surface area.[2] Further heat treatment at higher temperatures causes the framework structure to collapse resulting in a decrease in surface area.

The pore size distribution of the mesoporous material prepared at surfactant/$NiSO_4$ = 0.2 and Si/Ni = 0.21 is shown in Figure 10. It shows that even after heat treatment at 800 °C for 2 h, the mesophase still maintains a narrow pore size distribution with a specific surface area of 400 $m^2$/g. The average pore size of the mesophase as a function of treatment temperature is shown in Table 2.

Figure 11 shows the infrared absorption (IR) spectra of amorphous silica without $NiSO_4$, the nickel oxide without sodium silicate (surfactant/$NiSO_4$ = 0.2, Si/Ni = 0), and the nickel oxide−silicon oxide mesophase (surfactant/$NiSO_4$ = 0.2, Si/Ni = 0.21). All three samples had been calcined at 500 °C for 2 h. Comparing the absorption spectra in the neighborhood of wavenumber 1000 $cm^{-1}$ of the three materials, it is found that the mesophase has an additional peak at 1025 $cm^{-1}$. This additional peak is speculated to correspond to the bending motion of Si−O−Ni bond. There has been speculation of the existence of a Si−O−Ni bond.[20] However, no direct evidence has been shown in the literature.

## Conclusion

It is shown that mesostructured nickel silicate can be synthesized with $NiSO_4$, CTAB surfactant, and sodium silicate. The addition of sodium silicate in the precursor solution strengthens the mesostructure, which survived after heat treatment up to 800 °C. The amount of Si added must be higher than a threshold which depends on the surfactant/Si molar ratio. TEM shows that the mesophase is a disordered phase with uniform pore size. The mesophase has a composition of Si/Ni ≈ 0.5. Specific surface area as high as 530 $m^2$/g has been obtained in the current study.

## Acknowledgment

X. Liu and W.-H. Shih thank the partial support of DOE grant DE-FG22-94PC94215. The authors thank the support of Army Research Office, Multidisciplinary University Research Initiative under grant DAAH04-95-1-0102. We also thank Professor Yen Wei and Dr. Danliang Jin of the Chemistry Department at Drexel University for their help in the IR and TGA measurements.

## Literature Cited

(1) Beck, J. S.; Vartuli, J. C.; Roth, W. J.; Leonowicz, M. E.; Kresge, C. T.; Schmitt, K. D.; Chu, C. T.-W.; Olson, D. H.; Shepard, E. W.; McCullen, S. B.; Higgins, J. B.; Schlenker, J. L. A New Family of Mesoporous Molecular Sieves Prepared with Liquid Crystal Templates. *J. Am. Chem. Soc.* **1992**, *114*, 10834. Kresge, C. T.; Leonowicz, M. E.; Roth, W. J.; Vartuli, J. C.; Beck, J. S. Ordered Mesoporous Molecular Sieves Synthesized by a Liquid-Crystal Template Mechanism. *Nature* **1992**, *359*, 710.

(2) Chen, C.-Y.; Li, H.-X.; Davis, M. E. Studies on Mesoporous Materials, I. Synthesis and Characterization of MCM-41. *Microporous Mater.* **1993**, *2*, 17−26.

(3) Tanev, P. T.; Pinnavaia, T. J. A Neutral Templating Route to Mesoporous Molecular Sieves. *Science* **1995**, *267*, 865−867.

(4) Huo, Q.; Margolese, D. I.; Ciesla, U.; Feng, P.; Gier, T. E.; Sieger, P.; Leon, R.; Petroff, P. M.; Schuth, F.; Stucky, G. D. Generalized Synthesis of Periodic Surfactant/Inorganic Composite Materials. *Nature* **1994**, *368*, 317−321.

(5) Bagshaw, S. A.; Prouzet, E.; Pinnavaia, T. J. Templating of Mesoporous Molecular Sieves by Nonionic Poly(ethylene oxide) Surfactants. *Science* **1995**, *269*, 1242−1244.

(6) Tanev, P. T.; Pinnavaia, T. J. Mesoporous Silica Molecular Sieves Prepared by Ionic and Neutral Surfactant Templating: A Comparison of Physical Properties. *Chem. Mater.* **1996**, *8*, 2068−2079.

(7) Abe, T.; Taguchi, A.; Iwamoto, M.; Non-silica-Based Mesostructured Materials, 1. Synthesis of Vanadium Oxide-Based Material. *Chem. Mater.* **1995**, *7*, 1429−1430.

(8) Antonelli, D. M.; Ying, J. Y. Synthesis of Hexagonally Packed Mesoporous $TiO_2$ by a Modified Sol−Gel Method. *Angew. Chem.* **1995**, *34*, 2014.

(9) Liu, P. J.; Reddy, S.; Adnot, A.; Sayari, A. Mesostructured Zirconium Oxide. *Mater. Res. Soc. Symp. Proc.* **1996**, *431*, 101−110.

(10) Antonelli, D. M.; Ying, J. Y. Synthesis and Characterization of Hexagonally Packed Mesoporous Tantalum Oxide Molecular Sieves. *Chem. Mater.* **1996**, *8*, 874−881.

(11) Liu, P.; Liu, J.; Sayari, A. Preparation of Porous Hafnium Oxide in the Presence of a Cationic Surfactant. *Chem. Commun.* **1997**, *6*, 577−578.

(12) Antonelli, D. M.; Nakahira, A.; Ying, J. Y. Ligand-Assisted Liquid Crystal Templating in Mesoporous Niobium Oxide. *Inorg. Chem.* **1996**, *35*, 3126−3136.

(13) Tian, Z.-R.; Tong, W.; Wang, J.-Y.; Duan, N.-G.; Krishnan, V. V.; Suib, S. L. Maganese Oxide Mesoporous Structures: Mixed-Valence Semiconducting Catalysts. *Science* **1997**, *276*, 926−930.

(14) Vaudry, F.; Khodabandeh, S.; Davis, M. E. Synthesis of Pure Alumina Mesoporous Materials. *Chem. Mater.* **1996**, *8*, 1451−1464.

(15) Yada, M.; Machida, M.; Kijima, T. Synthesis and Reorganization of an Aluminum-Based Dodecyl Sulfate Mesophase with a Hexagonal Structure. *Chem. Commun.* **1996**, 769.

(16) Liu, K.-C.; Anderson, M. A. Porous Nickel Oxide/Nickel Films for Electrochemical Capacitors. *J. Electrochem. Soc.* **1996**, *143*, 124−130.

(17) Stein, A.; Fendorf, M.; Jarvie, T. P.; Mueller, K. T.; Benesi, A. J.; Mallouk, T. E. Salt−Gel Synthesis of Porous Transition-Metal Oxides. *Chem. Mater.* **1995**, *7*, 304−313.

(18) Brunauer, S.; Emmet, P. H.; Teller, E. Adsorption of Gases in Multimolecular Layers. *J. Am. Chem. Soc.* **1938**, *60*, 309.

(19) Barret, E. P.; Joyner, L. G.; Halenda, P. H. The Determination of Pore Volume and Area Distributions in Porous Substances. I. Computations from Nitrogen Isotherms. *J. Am. Chem. Soc.* **1951**, *73*, 373.

(20) Ramesh, S.; Koltypin, Y.; Prozorov, R.; Gedanken, A. Sonochemical Deposition and Characterization of Nanophasic Amorphous Nickel on Silica Microspheres. *Chem. Mater.* **1997**, *9*, 546−551.

*Received for review* February 22, 1999
*Revised manuscript received* August 16, 1999
*Accepted* August 16, 1999

IE990129L